Size Effect on Chemical Tuning of Spin−Lattice Relaxation Dynamics in Superparamagnetic Nanocrystals

Tai-Yen Chen, Chih-Hao Hsia, Hsiang-Yun Chen, and Dong Hee Son*

Department of Chemistry, Texas A&M University, College Station, Texas 77842

Received: April 20, 2010

The size-dependent chemical tunability of spin−lattice relaxation rate in magnetic nanocrystals has been investigated in size and composition-controlled colloidal superparamagnetic $Co_xFe_{3-x}O_4$ nanocrystals employing pump−probe Faraday rotation measurements. With the increase of cobalt content in $Co_xFe_{3-x}O_4$ nanocrystals, spin−lattice relaxation rate increased due to the increasing spin−orbit coupling strength regardless of the particle size. However, the range of the chemical tunability of spin−lattice relaxation was narrower in the smaller nanocrystals and the size dependence of spin−lattice relaxation rate became weaker with increasing cobalt content. These observations were explained in terms of weaker chemical tunability of spin−orbit coupling on the surface than in the interior of the nanocrystals using a simple model for spin−lattice relaxation rate that has both surface and interior contributions.

1. Introduction

Dynamics of spin relaxation in magnetic materials is a topic of active investigations in magnetism research in recent years.[1−3] The rate of energy and momentum flow between the spin and lattice, determining the time evolution of the magnetization, is not only of fundamental interest in the study of magnetism but also has a strong technological relevance in the application of magnetic materials in spin-based electronic or data storage devices.[4−6]

One of the key factors determining the rate of energy flow from spin to lattice degrees of freedom, i.e., spin−lattice relaxation, is spin−orbit coupling,[7,8] which can often be tuned by varying the stoichiometry of the materials. For example, the average spin−orbit coupling in ferrites ($M_xFe_{3-x}O_4$, M = divalent metal ion) can be tuned by varying the identity and composition of M.[9,10] Earlier studies on the dynamics of spin−lattice relaxation and its correlation to the structure of the magnetic materials have focused primarily on bulk and thin film phases.[11−14] Recently, interests in the dynamic magnetism in nanoscale magnetic materials have been growing rapidly,[3] since the reduction in length scale generally has a strong influence on the dynamics of energy relaxation in various degrees of freedom.[15]

The dynamics of energy relaxation in nanoscale materials has been well-studied for the electronic relaxation in semiconductors and metals, where the quantum confinement in combination with the large surface area plays a critical role in modifying the dynamics.[16−18] In the case of spin−lattice relaxation in magnetic materials, a large portion of the surface in nanocrystals can also influence the dynamics of spin−lattice relaxation due to the potentially different spin−orbit coupling or (and) vibronic coupling from the bulk. Recently, our group reported the observation of the size-dependent spin−lattice relaxation rate in Fe_3O_4 nanocrystals, where the rate became faster with the decreasing particle size.[19,20] The faster spin−lattice relaxation in the smaller nanocrystals was ascribed to the stronger spin−orbit coupling on the surface due to the generally weaker ligand field on the surface that enhances the effective spin−orbit coupling strength compared to the bulk.

One interesting question that arises from this earlier study is whether the relative efficiency of the surface of the nanocrystals in spin−lattice relaxation will vary with spin−orbit coupling of the bulk phase. An equivalent question from a different perspective is how the large surface area in nanocrystals would affect the chemical tunability of the spin−lattice relaxation rate.

In this report, we discuss the chemical tunabililty of the spin−lattice relaxation rate in nanoscale magnetic materials using size and composition-controlled colloidal superparamagnetic $Co_xFe_{3-x}O_4$ nanocrystals as the model system. $Co_xFe_{3-x}O_4$ is particularly useful for the purpose of this study, since magnetocrystalline anisotropy reflecting the bulk spin−orbit coupling strength can be varied by ∼20-fold by tuning cobalt content (x) without changing the lattice structure and static magnetization significantly.[21−25] Furthermore, the highly dispersible nature of the superparamagnetic nanocrystals in liquid medium allows us to study the dynamic magnetism unaffected by the interparticle magnetic dipole−dipole interaction.[26] While superparamagnetism is less useful for device applications, fine-tunability of the size and stoichiometry of the nanocrystals offers a unique opportunity to obtain a useful insight into the dynamics of spin−lattice relaxation in nanoscale materials.

To measure the spin−lattice relaxation rate of $Co_xFe_{3-x}O_4$ nanocrystals, we employed the pump−probe Faraday rotation technique that allowed us to monitor the time-dependent magnetization with a very high time resolution (<100 fs). The results of this study indicate that the chemical tunability of the spin−lattice relaxation rate becomes weaker with decreasing particle size and that the size dependence of the spin−lattice relaxation rate becomes weaker with increasing bulk spin−orbit coupling. These observations were explained in terms of the weaker chemical tunability of spin−orbit coupling on the surface than in the interior of the nanocrystal using a simple model for spin−lattice relaxation that has both surface and interior contributions.

* To whom correspondence should be addressed. E-mail: dhson@mail.chem.tamu.edu. Phone: 979-458-2990.

10.1021/jp103568k © 2010 American Chemical Society
Published on Web 05/06/2010

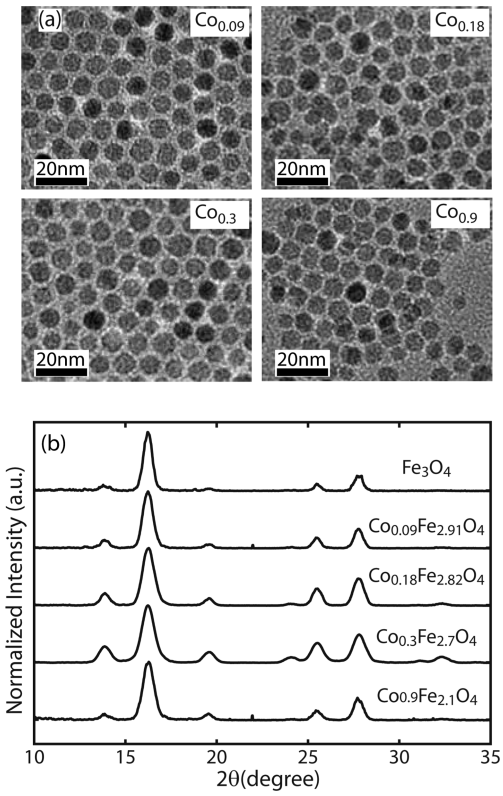

Figure 1. (a) Transmission electron micrographs of 7 nm $Co_xFe_{3-x}O_4$ nanocrystals. (b) X-ray diffraction pattern of 7 nm $Co_xFe_{3-x}O_4$ nanocrystals.

2. Experimental Section

Synthesis and Characterization of Nanocrystals. Spherical $Co_xFe_{3-x}O_4$ nanocrystals passivated with oleic acid with varying cobalt content (x) in the range of $0 < x < 0.9$ and diameter range of 5−15 nm were synthesized following the previously reported procedure and its variations.[27,28] For instance, 7 nm $Co_xFe_{3-x}O_4$ nanocrystals were synthesized by thermally decomposing iron acetylacetonate ($Fe(acac)_3$) and cobalt acetylacetonate ($Co(acac)_2$) with a mixture of oleic acid, oleylamine, and 1,2-dodecanediol at 290 °C in benzyl ether. Tuning of cobalt content was achieved by varying the molar ratio of $Fe(acac)_3$ and $Co(acac)_2$. $Co_xFe_{3-x}O_4$ nanocrystals of different diameters were prepared by varying the reaction temperature and time. The size and crystal structure of the nanocrystals were examined by transmission electron microscopy (TEM) and X-ray diffraction (XRD). Figure 1a shows the TEM images of 7 nm $Co_xFe_{3-x}O_4$ nanocrystals of varying cobalt content that exhibit less than 10% size dispersity. XRD patterns of all $Co_xFe_{3-x}O_4$ nanocrystals (Figure 1b) are very similar, consistent with the identical crystal structures (cubic inverse spinel) of Fe_3O_4 and $CoFe_2O_4$ with <0.2% difference in bulk lattice parameters: $a = 8.391$ and 8.381 Å for Fe_3O_4 and $CoFe_2O_4$, respectively.

Cobalt content (x) in $Co_xFe_{3-x}O_4$ nanocrystals was determined via elemental analysis of the nanocrystal samples employing inductively coupled plasma atomic emission spectroscopy (ICP-AES). For this measurement, dried $Co_xFe_{3-x}O_4$ nanocrystal samples were digested in 1 mL of aqueous (12 M) HCl solution. The solution further diluted to a ppm level of metal ion concentration in 1% aqueous HNO_3 solution was used to measure both Fe and Co ion concentrations.

Measurement of Static Mass Magnetization and Blocking Temperature. The static mass magnetization of $Co_xFe_{3-x}O_4$ nanocrystal samples was measured by using a superconducting quantum interference device (SQUID) magnetometer (MPMS-XL, Quantum Design). Saturation magnetization of $Co_xFe_{3-x}O_4$ nanocrystal samples was obtained from the field-dependent magnetization measurement at the temperature of 5 K. Similar to the results from previous study, the saturation magnetization exhibited only a very weak dependence on cobalt content (<4%).[29] To estimate the magnetic anisotropy constant (K_{aniso}) of the nanocrystals, blocking temperature (T_B) was also obtained from the zero-field-cooled (ZFC) magnetization measurement within the temperature range of 10−300 K. In the ZFC curve, the temperature at which the magnetization reaches the maximum value was taken as T_B. The magnetic anisotropy constant (K_{aniso}), partially reflecting the strength of spin−orbit coupling, was obtained from $K_{aniso} = 25k_BT_B/V$, where k_B is the Boltzmann constant and V is the volume of the nanocrystal.[21] For all the SQUID measurements, the nanocrystal samples were dispersed in liquid eicosane to avoid the aggregation and subsequently solidified to prevent the agitation of the nanocrystals in the matrix during the measurements.

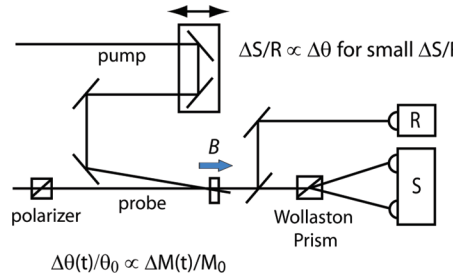

Figure 2. Experimental setup for pump−probe Faraday rotation measurement. The differential signal from balanced photodiode (ΔS) between with and without pump pulse normalized to the intensity of the probe beam (R) correcting for the absorption of probe by the sample is proportional to the differential Faraday rotation ($\Delta\theta$) between with and without pump for small values of $\Delta S/R$.

Time-Resolved Faraday Rotation Measurement. The spin−lattice relaxation rate in $Co_xFe_{3-x}O_4$ nanocrystals following an optical excitation was measured employing the pump−probe Faraday rotation technique. Faraday rotation is a magnetooptic technique that measures the relative magnitude of the magnetization indirectly from the rotation of the polarization angle of the linearly polarized light passing through the magnetic material. The Faraday rotation angle (θ) of the probe light is proportional to $M \cdot k$, where M is the magnetization vector of the sample and k is the wavevector of the probe light. In this work, the reduced magnetization of the nanocrystals by the absorption of the pump pulse recovers via spin−lattice relaxation. By measuring Faraday rotation as a function of the pump−probe time delay, $\theta(t)$, information on the time-dependent magnetization was obtained.[30]

Figure 2 shows the experimental setup employed in this study. Linearly polarized 790 nm pulses from an amplified titanium: sapphire laser (pulse width = 60 fs, repetition rate = 3 kHz, fwhm width = 150 μm) were used as the pump. Linearly polarized probe pulses in the visible or near-infrared regions were derived from the white light continuum generated by focusing 2 μJ of 790 nm pulse on a 1-mm-thick sapphire crystal. The time resolution of the measurement was ∼100 fs based on instrument limited signal rise time. The spectral bandwidth (20−30 nm fwhm) and wavelength of the probe beam were controlled by adjusting the width and the position of the slit in the prism dispersion compensator. A Glan linear polarizer was used to set the polarization angle of the probe light before it entered the sample. A Wollaston prism was placed after the sample, with its polarization axis set at 45° with respect to the

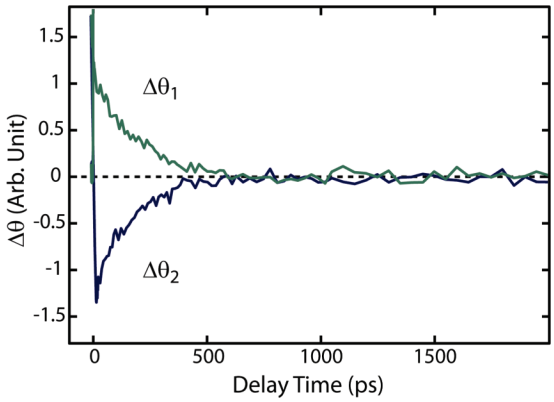

Figure 3. Pump−probe Faraday rotation data of 7 nm $Co_{0.9}Fe_{2.1}O_4$ nanocrystals under opposite external magnetic fields.

Glan polarizer. Faraday rotation was measured from the intensity difference between the two orthogonal polarization components of the probe light detected by a pair of balanced photodiodes. In this process, time-dependent absorption of the probe light by the sample was corrected for by simultaneously measuring the total intensity of the transmitted probe light. The external magnetic field of 0.35 T was provided by a pair of permanent magnets in the direction either parallel or antiparallel to the direction of the probe beam. Pump−probe Faraday rotation normalized to static Faraday rotation, $\Delta\theta(t)/\theta_0$, was taken to represent the time-dependent fractional changes in magnetization $|\Delta M(t)|/|M_0|$. To remove any potential nonmagnetic contribution to the Faraday rotation signal, the difference between the two data sets obtained with the magnetic fields parallel and antiparellel to the probe beam was taken to report $\Delta\theta(t)/\theta_0$.

For all the measurements, colloidal $Co_xFe_{3-x}O_4$ nanocrystal samples dispersed in 1-octadecene at room temperature were used. The sample solutions were continuously circulated at the linear speed of several meters/second through a jet nozzle (400 μm thick, 4 mm wide) to prevent a potential thermal effect and sample damage by the repeated exposure of the same sample region to the pump beam. The relatively high viscosity of 1-octadecene provided a sufficiently stable jet stream with a flat surface for the reliable measurements of Faraday rotation. The concentration of nanocrystals was maintained near 10^{-5} M or below to avoid interparticle dipole−dipole interaction that can potentially influence the dynamics.[26] Since the absorbance of $Co_xFe_{3-x}O_4$ nanocrystal samples at the pump wavelength (λ = 790 nm) varied slightly with cobalt content (Figure S1, Supporting Information), the pump fluence was adjusted to ensure the same average excitation density, i.e., number of photons absorbed per unit volume of nanocrystal, in all the measurements. All the fluence values reported here are the average fluence within the fwhm (30 μm) of the probe beam.

3. Results and Discussion

Measurement of Spin−Lattice Relaxation Rate of Spherical $Co_xFe_{3-x}O_4$ Nanocrystals. The spin−lattice relaxation rate of $Co_xFe_{3-x}O_4$ nanocrystals was obtained from the pump−probe Faraday rotation data showing the recovery of the magnetization following the optically induced demagnetization. Figure 3 shows the representative pump−probe Faraday rotation data from 7 nm $Co_{0.9}Fe_{2.1}O_4$ nanocrystals under the external magnetic field applied parallel ($\Delta\theta_1$) and antiparallel ($\Delta\theta_2$) to the direction of the probe beam. All the reported $\Delta\theta(t)/\theta_0$ data here were obtained from $\Delta\theta(t) = (\Delta\theta_2 - \Delta\theta_1)/2$ to remove the potential nonmagnetic component of the signal not sensitive to the polarity

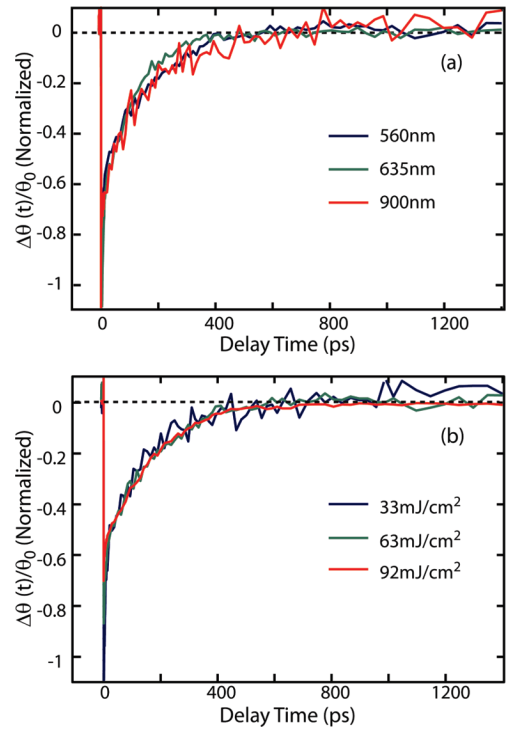

Figure 4. (a) Probe wavelength-dependent $\Delta\theta(t)/\theta_0$ of 7 nm $Co_{0.9}Fe_{2.1}O_4$ nanocrystals. (b) Excitation fluence-dependent $\Delta\theta(t)/\theta_0$ data normalized to pump fluence.

of the external magnetic field. The general feature of the pump−probe Faraday rotation data of $Co_xFe_{3-x}O_4$ nanocrystals is the immediate demagnetization by the absorption of the pump beam followed by the recovery of the magnetization. While the photoinduced ultrafast demagnetization in magnetic materials is also a topic of strong interest by itself,[11,31−33] we will mainly focus on the dynamics of the recovery of the magnetization occurring via spin−lattice relaxation in this study.

The time scale of spin−lattice relaxation (τ_{SLR}) was extracted by biexponetial fitting of $\Delta\theta(t)/\theta_0$ data. For all the data, the recovery of the signal could be fitted with two exponential time constants: ~10 ps and several hundreds of picoseconds. Such multiexponential recovery of magnetization has been previously observed in a number of ferromagnetic thin films.[12,34,35] Here, the recovery of $\Delta\theta(t)/\theta_0$ on the time scale of hundreds of picoseconds is of interest, which is ascribed to spin−lattice relaxation. The origin of the dynamics on ~10 ps time scale, on the other hand, is less clear although the dynamics on the short time scale has been previously associated with spin−spin relaxation between spin waves of different wavelengths in ferromagnetic metals.[36] Rotational diffusion of the nanocrystal in the solvent medium and directional fluctuation of magnetization is much slower than the time scale of the process we are interested in in this study and do not affect the dynamics reported here.[25]

To obtain a reliable spin−lattice relaxation rate of photoexcited $Co_xFe_{3-x}O_4$ nanocrystals, the Faraday rotation data were obtained at several different probe wavelengths and excitation fluences to check the consistency of the dynamics. Figure 4a shows $\Delta\theta(t)/\theta_0$ data from 7 nm $Co_{0.9}Fe_{2.1}O_4$ nanocrystals probed at three different wavelengths, λ = 560, 635, and 900 nm. The dynamics represented in these data do not exhibit significant spectral dependence as expected from $\Delta\theta(t)/\theta_0$ representing the magnetization dynamics.[14]

To avoid potential alteration of the dynamics of magnetization recovery by the heated lattice, the dependence of $\Delta\theta(t)/\theta_0$ on

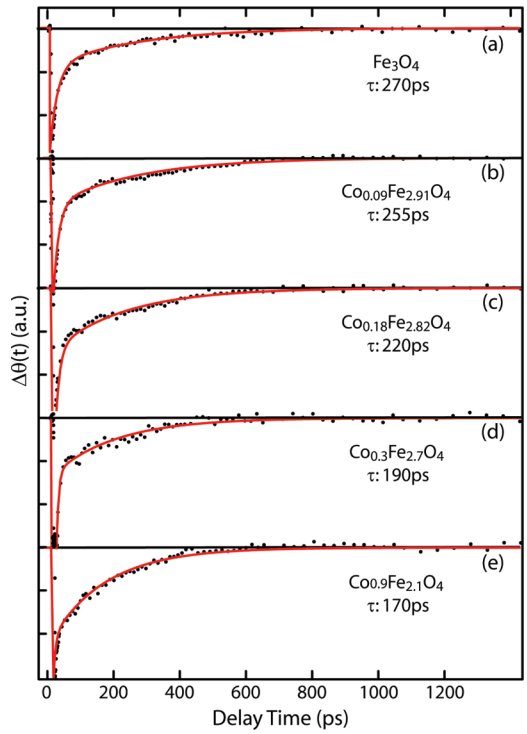

Figure 5. Cobalt content-dependent $\Delta\theta(t)$ data of 7 nm $Co_xFe_{3-x}O_4$ nanocrystals, $x = 0$, 0.09, 0.18, 0.3, and 0.9 for panels a to e, respectively.

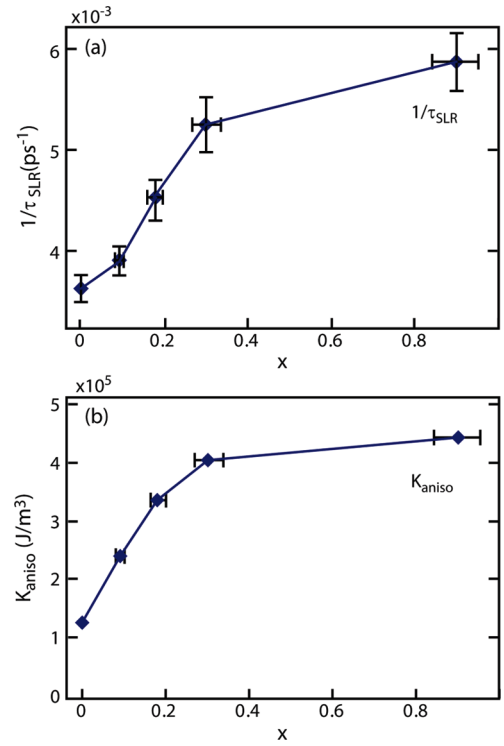

Figure 6. (a) Spin−lattice relaxation rate ($1/\tau_{SLR}$) and (b) magnetic anisotropy constant (K_{aniso}) of 7 nm $Co_xFe_{3-x}O_4$ nanocrystals as a function of cobalt content (x).

the excitation intensity was also checked. Figure 4b shows $\Delta\theta(t)/\theta_0$ data from 7 nm $Co_{0.9}Fe_{2.1}O_4$ nanocrystals at three different excitation fluences normalized to the excitation fluence. At these fluences, the amplitudes of the signal increased linearly to the excitation fluence and were almost identical when normalized to the excitation fluence. At higher excitation fluences, however, peak amplitude near zero time delay began to saturate and exhibited a nonmonotonic recovery dynamics. (Data not shown.) In this study, the excitation fluence was maintained on the low side of the linear regime (<50 mJ/cm^2) to avoid any potential complications by the heated lattice. According to our earlier study on the transient lattice temperature in photoexcited Fe_3O_4 nanocrystals, the initial temperature rise a few picoseconds after the excitation at the pump fluence of this study was <100 K and became <50 K within 100 ps in 7 nm nanocrystals.[37] Insensitivity of the dynamics to the pump fluence shown in Figure 4b suggests that the relatively low temperature rise and fast cooling of the lattice combined with high Curie temperature of $Co_xFe_{3-x}O_4$ does not affect the dynamics of the magnetization recovery. In this study, all the reported spin−lattice relaxation rates are the average of the values obtained from the measurements at these probe wavelengths and at the excitation fluence of <50 mJ/cm^2.

Chemical Tuning of Spin−Lattice Relaxation Rate of $Co_xFe_{3-x}O_4$ Nanocrystals. To investigate the effect of varying cobalt content (x) on spin−lattice relaxation rate and examine the correlation with spin−orbit coupling, the pump−probe Faraday rotation data of $Co_xFe_{3-x}O_4$ nanocrystal samples were obtained in the range of $0 < x < 0.9$. Figure 5a−e shows $\Delta\theta(t)/\theta_0$ data of 7 nm $Co_xFe_{3-x}O_4$ nanocrystals measured with 790 nm pump and 635 nm probe. Spin−lattice relaxation time (τ_{SLR}) obtained as described in the previous section is also displayed for each value of x. Figure 6a shows the spin−lattice relaxation rate ($1/\tau_{SLR}$) as a function of x. As cobalt content increases from $x = 0$ to 0.9, $1/\tau_{SLR}$ also increases by ~60%. On the other hand, transient absorption dynamics did not exhibit significant dependence on cobalt content, suggesting relatively week influence of cobalt substitution on the dynamics of electronic relaxation (Figure S2, Supporting Information).

In principle, the dependence of τ_{SLR} on cobalt content can originate from the differences in both spin−orbit coupling and vibronic coupling, since spin−lattice relaxation requires both of them. Because $CoFe_2O_4$ and Fe_3O_4 have very similar lattice structures, heat capacities, and vibrational spectra,[21−23] while their bulk magnetocrystalline anisotropies are different by a factor of ~20 ($1.1−1.3 \times 10^4$ J/m^3 for Fe_3O_4, $1.8−3.0 \times 10^5$ J/m^3 for $CoFe_2O_4$),[24,25] x-dependent τ_{SLR} observed in $Co_xFe_{3-x}O_4$ nanocrystals can be ascribed mainly to the differences in spin−orbit coupling.

To further examine the connection between the spin−lattice relaxation rate ($1/\tau_{SLR}$) with spin−orbit coupling of $Co_xFe_{3-x}O_4$ nanocrystals, x-dependence of magnetic anisotropy (K_{aniso}) is also measured as shown in Figure 6b. For bulk magnetic materials, magnetocrystalline anisotropy (K_{mca}) reflecting the strength of spin−orbit coupling of the bulk is the dominating component of the total magnetic anisotropy (K_{aniso}). In materials with simple uniaxial anisotropy, K_{mca} essentially represents the difference in spin−orbit energy between the direction of easy and hard axes, which is quadratically proportional to spin−orbit coupling.[38] For this reason, the spin−lattice relaxation rate of bulk magnetic materials was often correlated with K_{mca} in the earlier studies. In this study, we will use K_{aniso} as only an approximate parameter reflecting average spin−orbit coupling strength in $Co_xFe_{3-x}O_4$ nanocrystals as will be discussed further in detail later.

In panels a and b of Figure 6, both $1/\tau_{SLR}$ and K_{aniso} exhibit a similar trend, including the initial increase in the range of $0 < x < 0.3$ and subsequent saturation at higher values of x. This resemblance strongly indicates that the variation of spin−lattice relaxation rate is correlated with x-dependent spin−orbit

TABLE 1: Spin−Lattice Relaxation Rates ($1/\tau_{SLR}$, 10^{-3} ps^{-1}) of $Co_xFe_{3-x}O_4$ Nanocrystals

	x					
diameter (nm)	0	0.09	0.18	0.3	0.53	0.9
5	3.9 ± 0.1					
7	3.6 ± 0.1	3.9 ± 0.1	4.5 ± 0.2	5.3 ± 0.3	5.5 ± 0.3	5.8 ± 0.3
9	3.4 ± 0.1					
10	3.1 ± 0.1	3.9 ± 0.1		4.8 ± 0.2	5.2 ± 0.3	5.5 ± 0.3
15	2.9 ± 0.1				5.0 ± 0.3	

coupling strength in $Co_xFe_{3-x}O_4$ nanocrystals. However, K_{aniso} should be taken more cautiously as a measure of the average spin−orbit coupling strength of $Co_xFe_{3-x}O_4$ nanocrystals. In the case of nanocrystals, other contributing components to K_{aniso}, such as surface anisotropy (K_s), become significant and can even dominate in small nanocrystals. For spherical magnetic nanocrystals of diameter *d*, the following empirical relationship has often been used to describe K_{aniso}, although K_s is a more complex function of the surface and lattice structure in reality.

$$K_{aniso} = (K_{mca} + 6K_s/d) \quad (1)$$

The connection between surface anisotropy (K_s) and surface spin−orbit coupling is more complicated than in the bulk due to the complexity of the surface structure and symmetry that influences the surface anisotropy.[39,40] This introduces some uncertainty in K_{aniso} as the parameter representing the average spin−orbit coupling of the nanocrystals, making a quantitative correlation between K_{aniso} and $1/\tau_{SLR}$ more challenging in nanocrystals than in bulk. Nevertheless, the similarity of *x*-dependence of $1/\tau_{SLR}$ and K_{aniso} shown in panels a and b of Figure 6 clearly exhibits the tunability of the spin−lattice relaxation rate in nanocrystals via chemical tuning of the average spin−orbit coupling strength of the nanocrystals.

It is noteworthy to point out that the 60% change in spin−lattice relaxation rate observed in 7 nm $Co_xFe_{3-x}O_4$ nanocrystals within the range of $0 < x < 0.9$ in Figure 6a is narrower than what one might expect in the bulk phase. In the bulk phase of $Co_xFe_{3-x}O_4$, magnetocrystalline anisotropy increases by ~20-fold from Fe_3O_4 to $CoFe_2O_4$. According to the earlier studies on spin relaxation dynamics in thin films of chromium chalcogenides, the spin−lattice relaxation rate increased roughly linearly to bulk magnetocrystalline anisotropy although the correlation was crude.[41] In a recent study by Hübner et al., the spin−lattice relaxation rate in bulk metallic ferromagnets was predicted to be quadratically proportional to K_{mca} at high temperatures, while more comprehensive experimental verification has yet to be made.[8] Despite the uncertainties in the correlation between spin−orbit coupling and spin−lattice relaxation rate from the studies in bulk, the range of spin−lattice relaxation rates observed in $Co_xFe_{3-x}O_4$ nanocrystals still seems significantly narrower than that of K_{mca}.

This raises an interesting question on whether the chemical tuning of the spin−lattice relaxation rate is affected by the length scale of the materials. Considering our recent findings of the presence of the size effect on spin−lattice relaxation rate in Fe_3O_4 nanocrystals arising from the stronger spin−orbit coupling of the surface,[20] such a possibility is conceivable. To examine whether the range of chemical tuning in nanocrystals differs from that of the bulk, information on the spin−lattice relaxation rate in bulk $Co_xFe_{3-x}O_4$ is needed. Unfortunately, the data on the spin−lattice relaxation rate in the bulk phase required to make a direct comparison with the result from this work are not so far available. Although previous studies employing ferromagnetic resonance investigated the spin relaxation rate indirectly from the resonance line width, it was considered to reflect mostly spin−spin relaxation rather than spin−lattice relaxation.[42] Despite the lack of bulk data, a valuable insight can be obtained by comparing the spin−lattice relaxation rates in $Co_xFe_{3-x}O_4$ nanocrystals of varying particle sizes. In the next section, we will discuss how the chemical tuning of the spin−lattice relaxation is influenced by the size of the nanocrystals in more detail.

Size Effect on Chemical Tuning of Spin−Lattice Relaxation in $Co_xFe_{3-x}O_4$ Nanocrystals. To investigate the potential effect of varying the size on the chemical tuning of the spin−lattice relaxation rate in $Co_xFe_{3-x}O_4$ nanocrystals, more extensive measurements of *x*-dependent spin−lattice relaxation rate were made at varying particle sizes. The diameter of the spherical $Co_xFe_{3-x}O_4$ nanocrystal was varied in the range of 5−15 nm, while keeping all the samples below the superparamagnetic limit. The spin−lattice relaxation rates ($1/\tau_{SLR}$) of these nanocrystal samples measured under identical excitation densities are summarized in Table 1.

In Figure 7, the ranges of the chemical tuning of the spin−lattice relaxation rates of $Co_xFe_{3-x}O_4$ nanocrystals are compared for the two particle diameters, 7 and 10 nm. To delineate the difference more clearly, relative values of $1/\tau_{SLR}$ normalized to that of Fe_3O_4 nanocrystal samples are compared. For both sizes, the spin−lattice relaxation becomes faster with the increase of cobalt content. However, the ranges of the relative and absolute values of $1/\tau_{SLR}$ are larger in the larger nanocrystals. As cobalt content increased from $x = 0$ to 0.9, $1/\tau_{SLR}$ increased by 60% and 80% for 7 and 10 nm nanocrystals, respectively. The 15 nm nanocrystals follow the same trend between $x = 0$ and 0.53. This result indicates that the chemical tunability of the spin−lattice relaxation rate becomes weaker as the nanocrystal becomes smaller.

In Figure 8, the size dependence of the spin−lattice relaxation rate is compared for the two different cobalt contents, $x = 0$ and 0.53. To facilitate the comparison, the relative values of $1/\tau_{SLR}$ normalized to that of the 15 nm nanocrystal sample are plotted as a function of the diameter. The data indicate that

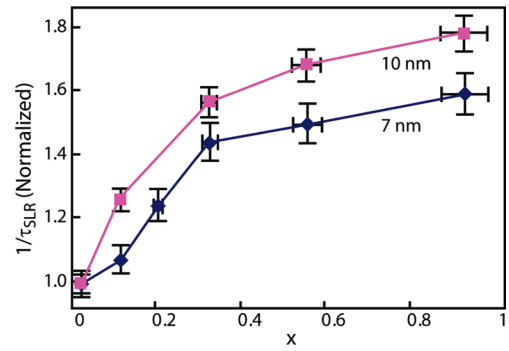

Figure 7. Comparison of the *x*-dependent relative spin−lattice relaxation rates of $Co_xFe_{3-x}O_4$ nanocrystals at two different particle diameters.

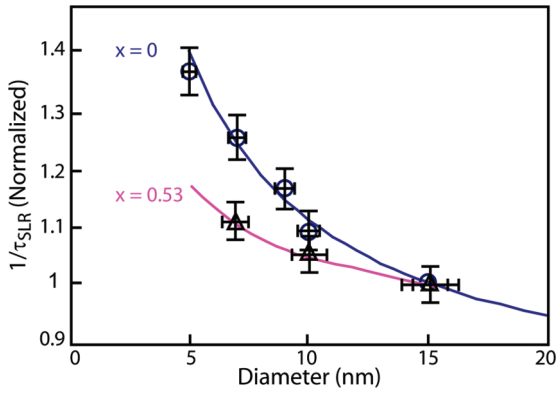

Figure 8. Comparison of the size-dependent relative spin−lattice relaxation rates of $Co_xFe_{3-x}O_4$ nanocrystals at two different cobalt contents.

$Co_xFe_{3-x}O_4$ nanocrystals with higher cobalt content, i.e., with stronger bulk spin−orbit coupling, exhibit the weaker dependence of the spin−lattice relaxation rate on the particle size.

These observations clearly indicate that varying cobalt content does not have the same effect on the spin−lattice relaxation of $Co_xFe_{3-x}O_4$ nanocrystals of different sizes. An insight into the size-dependent chemical tuning of the spin−lattice relaxation rate may be obtained by considering the role of surface in the spin−lattice relaxation of nanocrystals. In our earlier study in Fe_3O_4 nanocrystals, the spin−lattice relaxation rate was modeled to have contributions from both the interior ($|\langle V_i\rangle|^2$) and the surface ($|\langle V_s\rangle|^2$) proportionally to the fraction of the interior (f_i) and surface (f_s) spins.[20]

$$1/\tau_{SLR} \propto |\langle V\rangle|^2 = f_i|\langle V_i\rangle|^2 + f_s|\langle V_s\rangle|^2 \qquad (2)$$

Here, $|\langle V\rangle|^2$ is the coupling Hamiltonian term responsible for spin−lattice relaxation. From the analysis of $1/\tau_{SLR}$ vs diameter of Fe_3O_4 nanocrystals, it was concluded that the surface is 3 times more efficient than the interior of the nanocrystals in the spin−lattice relaxation, i.e., $|\langle V_s\rangle|^2/|\langle V_i\rangle|^2 = 3$.[20] When the same analysis is made on $Co_{0.53}Fe_{2.47}O_4$ nanocrystals, $|\langle V_s\rangle|^2/|\langle V_i\rangle|^2$ is 1.7. This suggests that the observed size dependence of the chemical tuning of the spin−lattice relaxation can be explained if $|\langle V_s\rangle|^2$ is less chemically sensitive than $|\langle V_i\rangle|^2$. In such a situation, the range of chemical tuning of the spin−lattice relaxation will become smaller as the contribution of the surface to the overall spin−lattice relaxation increases. One would also expect weaker size dependence of the spin−lattice relaxation rate with increasing bulk spin−orbit coupling due to the decreasing contribution of the surface in determining the overall spin−lattice relaxation rate. Since the electronic relaxation rate of $Co_xFe_{3-x}O_4$ nanocrystals through vibronic coupling is not sensitive to cobalt content, the weaker chemical tunability of $|\langle V_s\rangle|^2$ can be interpreted as the weaker tunability of spin−orbit coupling on the surface.

The relatively weak chemical tunability of spin−orbit coupling on the surface compared to the interior of the nanocrystals could arise from different causes. For instance, inhomogeneous distribution of cobalt ions with preferential occupation in the interior region of the nanocrystal may weaken the chemical sensitivity of surface spin−orbit coupling. We do not think this is a likely situation, since cobalt ions are considered to distribute homogeneously in the nanocrystals prepared at the high reaction temperatures of this study (290 °C).[43] On the other hand, a more complex ligand field on the surface could diminish the chemical sensitivity of the effective surface spin−orbit coupling, since the ligand field is another important factor affecting the effective spin−orbit coupling in crystalline materials. While further studies are needed for more direct evidence for the weaker chemical sensitivity of surface spin−orbit coupling and its cause, this study offers a simple framework to interpret the size and stoichiometry-dependent spin−lattice relaxation rates in superparamagnetic nanocrystals.

4. Conclusion

In summary, the chemical tunability of spin−lattice relaxation rates in colloidal superparamagnetic $Co_xFe_{3-x}O_4$ nanocrystals was investigated at different particle sizes. With increasing cobalt content (x), the spin−lattice relaxation rate increases due to the increase in the spin−orbit coupling strength regardless of the particle size. However, the range of chemical tunability of the spin−lattice relaxation rate becomes narrower with the decreasing particle size. Furthermore, the size dependence of the spin−lattice relaxation rate becomes weaker as cobalt content increases in $Co_xFe_{3-x}O_4$ nanocrystals. These observations suggest that spin−orbit coupling of the surface is less sensitive to stoichiometric variation than the interior of the nanocrystals.

Acknowledgment. This work was supported by NSF CAREER (DMR-0845645). We thank Microscopy and Imaging Center, Material Characterization Facility, and Trace Elemental Laboratory of TAMU for TEM, UV−vis−NIR, and ICP-AES measurements. We also thank the department of chemistry SQUID facility of TAMU (NSF-9974899) for all SQUID measurements conducted in this work.

Supporting Information Available: UV−vis−NIR spectra and cobalt content-dependent transient absorption data of 7 nm $Co_xFe_{3-x}O_4$ nanocrystals. This material is available free of charge via the Internet at http://pubs.acs.org.

References and Notes

(1) Kimel, A. V.; Kirilyuk, A.; Usachev, P. A.; Pisarev, R. V.; Balbashov, A. M.; Rasing, T. Ultrafast Non-Thermal Control of Magnetization by Instantaneous Photomagnetic Pulses. *Nature* **2005**, *435*, 655–657.

(2) Müller, G. M.; Walowski, J.; Djordjevic, M.; Miao, G.-X.; Gupta, A.; Ramos, A. V.; Gehrke, K.; Moshnyaga, V.; Samwer, K.; Schmalhorst, J.; Thomas, A.; Hütten, A.; Reiss, G.; Moodera, J. S.; Münzenberg, M. Spin Polarization in Half-Metals Probed by Femtosecond Spin Excitation. *Nat. Mater.* **2009**, *8*, 56–61.

(3) Krivorotov, I. N.; Emley, N. C.; Sankey, J. C.; Kiselev, S. I.; Ralph, D. C.; Buhrman, R. A. Time-Domain Measurements of Nanomagnet Dynamics Driven by Spin-Transfer Torques. *Science* **2005**, *307*, 228–231.

(4) Chappert, C.; Fert, A.; van Dau, F. N. The Emergence of Spin Electronics in Data Storage. *Nat. Mater.* **2007**, *6*, 813–823.

(5) Wolf, S. A.; Awschalom, D. D.; Buhrman, R. A.; Daughton, J. M.; von Molnár, S.; Roukes, M. L.; Chtchelkanova, A. Y.; Treger, D. M. Spintronics: A Spin-Based Electronics Vision for the Future. *Science* **2001**, *294*, 1488–1495.

(6) Prinz, G. A. Magnetoelectronics. *Science* **1998**, *282*, 1660–1663.

(7) Stöhr, J.; Siegmann, H. C. *Magnetism: From Fundamentals to Nanoscale Dynamics*: Springer: Berlin, Germany, 2006.

(8) Hübner, W.; Bennemann, K. H. Simple Theory for Spin−Lattice Relaxation in Metallic Rare-Earth Ferromagnets. *Phys. Rev. B* **1996**, *53*, 3422–3427.

(9) Penoyer, R. F.; Bickford, L. R. Magnetic Annealing Effect in Cobalt-Substituted Magnetite Single Crystals. *Phys. Rev.* **1957**, *108*, 271–277.

(10) Tachiki, M. Origin of the Magnetic Anisotropy Energy of Cobalt Ferrite. *Prog. Theor. Phys.* **1960**, *23*, 1055–1072.

(11) Beaurepaire, E.; Merle, J. C.; Daunois, A.; Bigot, J.-Y. Ultrafast Spin Dynamics in Ferromagnetic Nickel. *Phys. Rev. Lett.* **1996**, *76*, 4250–4253.

(12) Djordjevic, M.; Lüttich, M.; Moschkau, P.; Guderian, P.; Kampfrath, T.; Ulbrich, R. G.; Münzenberg, M.; Felsch, W.; Moodera, J. S. Comprehensive View on Ultrafast Dynamics of Ferromagnetic Films. *Phys. Status Solidi C* **2006**, *3*, 1347–1358.

(13) Zhang, Q.; Nurmikko, A. V.; Miao, G. X.; Xiao, G.; Gupta, A. Ultrafast Spin-Dynamics in Half-Metallic CrO_2 Thin Films. *Phys. Rev. B* **2006**, *74*, 064414.

(14) Bigot, J.-Y.; Guidoni, L.; Beaurepaire, E.; Saeta, P. N. Femtosecond Spectrotemporal Magneto-Optics. *Phys. Rev. Lett.* **2004**, *93*, 077401.

(15) Awschalom, D. D.; DiVincenzo, D. P.; Smyth, J. F. Macroscopic Quantum Effects in Nanometer-Scale Magnets. *Science* **1992**, *258*, 414–421.

(16) Klimov, V. I.; McBranch, D. W. Femtosecond 1P-to-1S Electron Relaxation in Strongly Confined Semiconductor Nanocrystals. *Phys. Rev. Lett.* **1998**, *80*, 4028–4031.

(17) Burda, C.; Chen, X.; Narayanan, R.; El-Sayed, M. A. Chemistry and Properties of Nanocrystals of Different Shapes. *Chem. Rev.* **2005**, *105*, 1025–1102.

(18) Cooney, R. R.; Sewall, S. L.; Dias, E. A.; Sagar, D. M.; Anderson, K. E. H.; Kambhampati, P. Unified Picture of Electron and Hole Relaxation Pathways in Semiconductor Quantum Dots. *Phys. Rev. B* **2007**, *75*, 245311.

(19) Hsia, C.-H.; Chen, T.-Y.; Son, D. H. Size-Dependent Ultrafast Magnetization Dynamics in Iron Oxide (Fe_3O_4) Nanocrystals. *Nano Lett.* **2008**, *8*, 571–576.

(20) Hsia, C.-H.; Chen, T.-Y.; Son, D. H. Time-Resolved Study of Surface Spin Effect on Spin−Lattice Relaxation in Fe_3O_4 Nanocrystals. *J. Am. Chem. Soc.* **2009**, *131*, 9146–9147.

(21) Cullity, B. D. *Introduction to Magnetic Materials*; Addison-Wesley Pub. Co.: Reading, MA, 1972; p 190.

(22) Ziemniak, S. E.; Anovitz, L. M.; Castelli, R. A.; Porter, W. D. Magnetic Contribution to Heat Capacity and Entropy of Nickel Ferrite ($NiFe_2O_4$). *J. Phys. Chem. Solids* **2007**, *68*, 10–21.

(23) Wohlfarth, E. P. *Ferromagnetic Materials: A Handbook on the Properties of Magnetically Ordered Substances*: North-Holland: New York, 1986; Vol. 3, pp 286−289.

(24) Goya, G. F.; Berquó, T. S.; Fonseca, F. C.; Morales, M. P. Static and Dynamic Magnetic Properties of Spherical Magnetite Nanoparticles. *J. Appl. Phys.* **2003**, *94*, 3520–3528.

(25) Adam, J. R.; Anna, C. S. S.; Zhang, Z. J. Characterizing the Magnetic Anisotropy Constant of Spinel Cobalt Ferrite Nanoparticles. *Appl. Phys. Lett.* **2000**, *76*, 3624–3626.

(26) Vestal, C. R.; Song, Q.; Zhang, Z. J. Effects of Interparticle Interactions upon the Magnetic Properties of $CoFe_2O_4$ and $MnFe_2O_4$ Nanocrystals. *J. Phys. Chem. B* **2004**, *108*, 18222–18227.

(27) Sun, S.; Zeng, H. Size-Controlled Synthesis of Magnetite Nanoparticles. *J. Am. Chem. Soc.* **2002**, *124*, 8204–8205.

(28) Sun, S.; Zeng, H.; Robinson, D. B.; Raoux, S.; Rice, P. M.; Wang, S. X.; Li, G. Monodisperse MFe_2O_4 (M = Fe, Co, Mn) Nanoparticles. *J. Am. Chem. Soc.* **2003**, *126*, 273–279.

(29) Song, Q.; Zhang, Z. J. Correlation between Spin-Orbital Coupling and the Superparamagnetic Properties in Magnetite and Cobalt Ferrite Spinel Nanocrystals. *J. Phys. Chem. B* **2006**, *110*, 11205–11209.

(30) Lifshitz, E. M.; Landau, L. D.; Pitaevskii, L. P. *Electrodynamics of Continuous Media*; Pergamon Press: New York, 1984.

(31) Stamm, C.; Kachel, T.; Pontius, N.; Mitzner, R.; Quast, T.; Holldack, K.; Khan, S.; Lupulescu, C.; Aziz, E. F.; Wietstruk, M.; Dürr, H. A.; Eberhardt, W. Femtosecond Modification of Electron Localization and Transfer of Angular Momentum in Nickel. *Nat. Mater.* **2007**, *6*, 740–743.

(32) Zhang, G. P.; Hübner, W. Laser-Induced Ultrafast Demagnetization in Ferromagnetic Metals. *Phys. Rev. Lett.* **2000**, *85*, 3025–3028.

(33) Koopmans, B.; Ruigrok, J. J. M.; Longa, F. D.; de Jonge, W. J. M. Unifying Ultrafast Magnetization Dynamics. *Phys. Rev. Lett.* **2005**, *95*, 267207.

(34) Kise, T.; Ogasawara, T.; Ashida, M.; Tomioka, Y.; Tokura, Y.; Kuwata-Gonokami, M. Ultrafast Spin Dynamics and Critical Behavior in Half-Metallic Ferromagnet: Sr_2FeMoO_6. *Phys. Rev. Lett.* **2000**, *85*, 1986–1989.

(35) Koopmans, B.; van Kampen, M.; Kohlhepp, J. T.; de Jonge, W. J. M. Ultrafast Magneto-Optics in Nickel: Magnetism or Optics. *Phys. Rev. Lett.* **2000**, *85*, 844–847.

(36) Djordjevic, M.; Münzenberg, M. Connecting the Timescales in Picosecond Remagnetization Experiments. *Phys. Rev. B* **2007**, *75*, 012404.

(37) Chen, T.-Y.; Hsia, C.-H.; Son, D. H. Time-Dependent Elastic Properties and Lattice Temperature of the Photoexcited Iron Oxide Nanocrystals. *J. Phys. Chem. C* **2008**, *112*, 10125–10129.

(38) Lessard, A.; Moos, T. H.; Hübner, W. Magnetocrystalline Anisotropy Energy of Transition-Metal Thin Films: A Nonperturbative Theory. *Phys. Rev. B* **1997**, *56*, 2594–2604.

(39) Morales, M. A.; Skomski, R.; Fritz, S.; Shelburne, G.; Shield, J. E.; Yin, M.; O'Brien, S.; Leslie-Pelecky, D. L. Surface Anisotropy and Magnetic Freezing of MnO Nanoparticles. *Phys. Rev. B* **2007**, *75*, 134423.

(40) Skomski, R.; Coey, J. M. D. *Permanent Magnetism*; Institute of Physics: Bristol, UK, 1999.

(41) Ogasawara, T.; Ohgushi, K.; Tomioka, Y.; Takahashi, K. S.; Okamoto, H.; Kawasaki, M.; Tokura, Y. General Features of Photoinduced Spin Dynamics in Ferromagnetic and Ferrimagnetic Compounds. *Phys. Rev. Lett.* **2005**, *94*, 087202.

(42) Sparks, M. *Ferromagnetic-Relaxation Theory*: McGraw-Hill: New York, 1964.

(43) Liu, C.; Zou, B.; Rondinone, A. J.; Zhang, Z. J. Chemical Control of Superparamagnetic Properties of Magnesium and Cobalt Spinel Ferrite Nanoparticles through Atomic Level Magnetic Couplings. *J. Am. Chem. Soc.* **2000**, *122*, 6263–6267.

JP103568K